

# Monte Carlo Simulation of Comptonization in Inhomogeneous Media

Xin-Min Hua<sup>1</sup>

Laboratory for High Energy Astrophysics, NASA/GSFC Code 661, Greenbelt, MD 20771

hua@rosserv.gsfc.nasa.gov

## ABSTRACT

Comptonization is the process in which photon spectrum changes due to multiple Compton scatterings in the electronic plasma. It plays an important role in the spectral formation of astrophysical X-ray and gamma-ray sources. There are several intrinsic limitations for the analytical method in dealing with the Comptonization problem and Monte Carlo simulation is one of the few alternatives. We describe an efficient Monte Carlo method that can solve the Comptonization problem in a fully relativistic way. We expanded the method so that it is capable of simulating Comptonization in the media where electron density and temperature varies discontinuously from one region to the other and in the isothermal media where density varies continuously along photon paths. The algorithms are presented in detail to facilitate computer code implementation. We also present a few examples of its application to the astrophysical research.

## 1. Introduction

Comptonization – the process where photon spectrum changes due to multiple Compton scatterings in the electronic plasma – is one of the most important processes in the spectral generation of X-ray binaries, active galactic nuclei and other X-ray and gamma-ray sources. The analytical treatment of Comptonization are essentially based on the solution of Kompaneets equation which describes the interactions between radiation field and thermal electrons (Kompaneets 1956). Due to the mathematical complexity, however, previous analysis of Comptonization depended on simplifications such as the non-relativistic approximation and therefore the results were only applicable to a relatively small range of photon and electron energies (e.g. Sunyaev & Titarchuk 1980). In recent years, Titarchuk (1994) developed a modified analytical technique which took into account the relativistic effect and Klein-Nishina corrections, thereby extending the previous work to wider ranges of temperature and optical depth of the plasma clouds from which Comptonized photons emerge.

---

<sup>1</sup>also Universities Space Research Association

The analytical method, however, have several intrinsic limitations. First, all analytical models are based on solving certain types of radiation transfer equations (Kompaneets 1956), which in turn is based on the assumption that energy and position of the photons are continuous functions of time, i.e. these models assume diffusion of photons in the energy and position spaces. While the continuity of energy change is a good approximation for scatterings at low energy, it is obviously not valid for Compton scatterings at high photon energies or by relativistic electrons. Similarly, the continuity of photon position change is an approximation only valid for clouds of electron plasma with dimensions large compared to the scattering mean free path (i.e. diffusion approximation). But astronomical observations suggest that many of the sources where Comptonization is believed to take place have optical depths of the order of one Thomson scattering mean free path.

Second, solutions of the radiative transfer equations are based on the separation of photon diffusions in energy and position spaces (Sunyaev & Titarchuk 1980, Titarchuk 1994 and Hua & Titarchuk 1995). The solutions can be presented in terms of simple analytical expressions only when initial source photons have energies much lower than the electron energy and follow a particular spatial distribution, namely, the first eigenfunction of the spatial operator of the diffusion equation. It was found (Hua & Titarchuk 1995) that for source photons at energies not far below the electron energy or for clouds with large optical depth, the emergent spectra are sensitive to both the spectral and spatial distributions of source photons and the results of analytical method must be expanded to the higher order terms. Consequently, the analytical models are applicable only to certain ranges of plasma temperature and optical depth where solutions are insensitive to source conditions.

Third, the analytical methods are inadequate to treat the temporal behavior of Comptonized emissions. Hua & Titarchuk (1996) have shown that for relativistic plasma, photons gain energy significantly with each scattering and consequently the scattering mean free path changes significantly with each scattering. Besides, for plasma clouds with small optical depth, the scattering mean free path are mainly determined by the boundary condition instead of the scattering cross sections. As a result, analytical treatment (e.g. Payne 1980), is only applicable to the limited situation in which electron plasma has non-relativistic temperatures and optical depths much greater than Thomson mean free path.

In addition to the above limitations, analytical approach is totally incapable of dealing with the Comptonization problems involving complicated geometries and inhomogeneity of electronic media, where scattering mean free path depends on scattering location and direction as well as photon energy. But observations seem to indicate that investigations of Comptonization in the media with non-uniform temperature and density are necessary. As was shown by Skibo et al. (1995) and Ling et al. (1997), the spectral hardening at high energies in the spectra of AGNs and black hole candidates may be resulting from the temperature gradient in the plasmas responsible for the emissions. Kazanas et al. (1997) and Hua et al. (1997) showed that the temporal behavior such as the hard X-ray phase lags observed from the accreting compact objects may be explained by the non-uniform electron density of the accreting gas clouds.

These situations are where analytical method fails. As an alternative, Monte Carlo simulation can be employed to give solutions. It is flexible in simulating various initial conditions of source photons, complicated geometries and density profiles of plasma clouds. It is capable of presenting the full spectra resulting from Comptonization rather than the asymptotic ones obtainable from analytical methods. The first attempt to use Monte Carlo method to solve Comptonization problem was by Pozdnyakov et al. (1983). In recent years, Stern et al. (1995) presented a large-particle Monte Carlo method for simulating Comptonization and other high-energy processes. Skibo et al. (1995) used a Monte Carlo simulation in the calculation of photon spectra of mildly relativistic thermal plasmas in pair balance.

In this study, we develop an efficient Monte Carlo method which treats Comptonization problem in a fully relativistic way and can be implemented in a medium computer such as Sparc workstation or Pentium PC to yield results with satisfactory statistics in CPU time of the order of minutes to hours. The algorithms are described in detail to facilitate computer code implementation. In §2 we introduce an improved technique of simulating Compton scattering of photons on cold electrons. In §3, we describe the method for Compton scattering on hot electrons. In §4, we present the method dealing with scattering in multi-zone medium. In §5, we describe the simulation of Compton scatterings in media with non-uniform density profiles.

## 2. Compton Scattering on Cold Electrons

The Monte Carlo method described here was developed over the past several years in the investigations of Compton scattering of 2.223 MeV gamma-ray line in solar flares (Hua 1986), Compton backscattering of 511 keV annihilation line in the sources 1E1740.7-2942 (Lingenfelter & Hua 1991) and Nova Muscae (Hua & Lingenfelter 1993).

The differential cross section of Compton scattering is given by the Klein-Nishina formula

$$\frac{d\sigma}{d\varepsilon} = \frac{3\sigma_T}{4} \cdot \frac{1}{\varepsilon} \left[ \left(1 - \frac{4}{\varepsilon} - \frac{8}{\varepsilon^2}\right) \ln(1 + \varepsilon) + \frac{1}{2} + \frac{8}{\varepsilon} - \frac{1}{2(1 + \varepsilon)^2} \right], \quad (1)$$

where  $\sigma_T$  is Thomson cross section;  $\varepsilon = 2E/m_e c^2$ ;  $E$  is the energy of incident photon;  $m_e$  is the electron rest mass and  $c$  the speed of light. The energy of the scattered photon,  $E'$ , relative to the initial photon energy  $E$  is given by the ratio

$$r = \frac{E}{E'} = 1 + \frac{\varepsilon}{2}(1 - \cos \psi), \quad (2)$$

where  $\psi$  is the angle between incident and scattered photons. The energy distribution of the Compton-scattered photons is determined by the distribution with respect to  $r$ , which is

$$f(r) = \begin{cases} \frac{1}{K(\varepsilon)} \left[ \left( \frac{\varepsilon + 2 - 2r}{\varepsilon r} \right)^2 + \frac{1}{r} - \frac{1}{r^2} + \frac{1}{r^3} \right] & \text{for } 1 \leq r \leq \varepsilon + 1, \\ 0 & \text{otherwise,} \end{cases} \quad (3)$$

where

$$K(\varepsilon) = \frac{4\varepsilon}{3\sigma_T}\sigma(\varepsilon) \quad (4)$$

is the normalization factor.

Sampling the distribution given by Eq. (3) plays a central role in the Monte Carlo simulation of Compton scattering of photons by cold electrons. Furthermore, as will be seen below, Compton scatterings on hot electrons in our scheme will also be reduced to the simulation of Eq. (3). Therefore, the performance of the computer program for Monte Carlo simulation of Compton scatterings depends critically on the quality of the technique used for sampling this distribution because a run of the program typically involves millions of scatterings. Efforts were made to optimize the technique of sampling this distribution (e.g. Kahn, 1954). In our implementation, we adopted a variation of Kahn’s technique first suggested by Pei (1979). The algorithm of the technique is

1. Generate 3 random numbers  $\xi_1, \xi_2$  and  $\xi_3$  uniformly distributed on (0,1).
2. If  $\xi_1 \leq 27/(2\varepsilon + 29)$ ,
  - let  $r = (\varepsilon + 1)/(\varepsilon\xi_2 + 1)$ .
  - If  $\xi_3 > \{[(\varepsilon + 2 - 2r)/\varepsilon]^2 + 1\}/2$ , go to 1.
  - Else accept  $r$ .
- Else
  - let  $r = \varepsilon\xi_2 + 1$ .
  - If  $\xi_3 > 6.75(r - 1)^2/r^3$ , go to 1.
  - Else accept  $r$ .

It is seen that this is essentially a combination of composition and rejection methods (see e.g. Ripley, 1987). This algorithm, like Kahn’s, avoids the operations such as square root, logarithm or trigonometric functions, which involve time-consuming series expansion for computers. Its quality can also be measured to a large extent by the rejection rates, which are 0.38, 0.30, 0.23 and 0.33 for  $\varepsilon = 0.2, 2, 10$  and  $20$  respectively, as compared to 0.41, 0.37, 0.41 and 0.53 for Kahn’s technique. The improvement is significant, especially for higher photon energies.

### 3. Comptonization in Hot Isothermal Homogeneous Plasmas

The Monte Carlo technique for photon Comptonization in a relativistic plasma was outlined by Pozdnyakov et al. (1983) and Gorecki & Wilczewski (1984). Our implementation of the simulation is somewhat different from these authors. It was developed on the bases of the technique for Compton scattering on cold electrons described in the last section.

Suppose a photon is scattered off an electron which is moving in  $z$ -axis direction with a velocity  $v$ . The energies of the incident and the scattered photon are  $E$  and  $E'$  respectively. The

zenith angles of the incident and scattered photons measured from  $z$ -axis are  $\theta$  and  $\theta'$  respectively.  $\phi$  and  $\phi'$  are the azimuthal angles. The differential cross section for Compton scattering is given by (see e.g. Akhiezer & Berestetskii 1969)

$$\frac{d\sigma}{d\mu'd\phi'} = \frac{3\sigma_T}{16\pi} \frac{1}{\gamma^2} \frac{\chi}{(1-v\mu)^2} \left(\frac{E'}{E}\right)^2, \quad (5)$$

where  $\mu = \cos\theta$  and  $\mu' = \cos\theta'$ ;  $v$  is in units of the speed of light and  $\gamma = (1-v^2)^{-1/2}$ ;

$$\chi = \frac{\varepsilon}{\varepsilon'} + \frac{\varepsilon'}{\varepsilon} + \frac{4}{\varepsilon} \left(1 - \frac{\varepsilon}{\varepsilon'}\right) + \frac{4}{\varepsilon^2} \left(1 - \frac{\varepsilon}{\varepsilon'}\right)^2; \quad (6)$$

$$\varepsilon = \frac{2E}{m_e c^2} \gamma (1 - v\mu), \quad \varepsilon' = \frac{2E'}{m_e c^2} \gamma (1 - v\mu'); \quad (7)$$

$$\frac{E'}{E} = \frac{1 - v\mu}{1 - v\mu' + (E/\gamma m_e c^2)(1 - \cos\psi)}; \quad (8)$$

and  $\psi$  is the angle between incident and scattered photons  $\cos\psi = \mu\mu' + \sqrt{(1-\mu^2)(1-\mu'^2)} \cos(\phi - \phi')$ .

Integration over  $\mu'$  and  $\phi'$  leads to

$$\sigma(\varepsilon) = \frac{3\sigma_T}{4} \cdot \frac{1}{\varepsilon} \left[ \left(1 - \frac{4}{\varepsilon} - \frac{8}{\varepsilon^2}\right) \ln(1 + \varepsilon) + \frac{1}{2} + \frac{8}{\varepsilon} - \frac{1}{2(1 + \varepsilon)^2} \right]. \quad (9)$$

It is seen that Eq. (9) is identical in form with Eq. (1). But the quantity  $\varepsilon$  here is given by the relativistic expression in Eq. (7). In other words, it is dependent on the electron's energy and direction as well as photon's energy.

A photon with energy  $E$  traveling in a plasma with an isotropic distribution of electrons having an energy distribution  $N_e(\gamma)$  will have an averaged cross section of Compton scattering (see e.g. Landau & Lifshits, 1976):

$$\sigma_a(T_e, E) = \frac{1}{2} \int_1^\infty d\gamma \int_{-1}^1 d\mu (1 - v\mu) \sigma(\varepsilon) N_e(\gamma). \quad (10)$$

For a plasma in thermal equilibrium,  $N_e(\gamma)$  is the Maxwell distribution given by

$$N_e(\gamma) = \frac{1}{2\Theta K_2(1/\Theta)} v \gamma^2 e^{-\gamma/\Theta}, \quad (11)$$

where  $\Theta = kT_e/m_e c^2$  is the dimensionless temperature of the plasma;  $k$  is the Boltzmann constant and  $K_2$  is the modified Bessel function of 2nd order. The  $\sigma_a(T_e, E)$  values in the form of a data matrix, obtained by the 2-dimensional integration in Eq. (10) for a properly spaced array of  $T_e$  and  $E$ , can be read by or incorporated into the computer codes. Values of  $\sigma_a(T_e, E)$  for several

temperatures are numerically calculated and plotted in Figure 1. The dashed curve in the figure is the cross section at  $T_e = 0$ , given by the Klein-Nishina formula in Eq. (1). It can be seen that for energetic photons scattering off the high temperature electrons, the cross section can be smaller by a factor of 2 or more than off the cold electrons. In other words, hot plasmas are more transparent than cold ones for photons. This has important effect on the energy spectra emerging from such plasmas, which Titarchuk (1994) took into account in his modification of the previous analytical results. Its effect on the temporal behavior of X-ray and gamma-ray emission from these plasma is even more significant and was discussed in Hua & Titarchuk (1996).

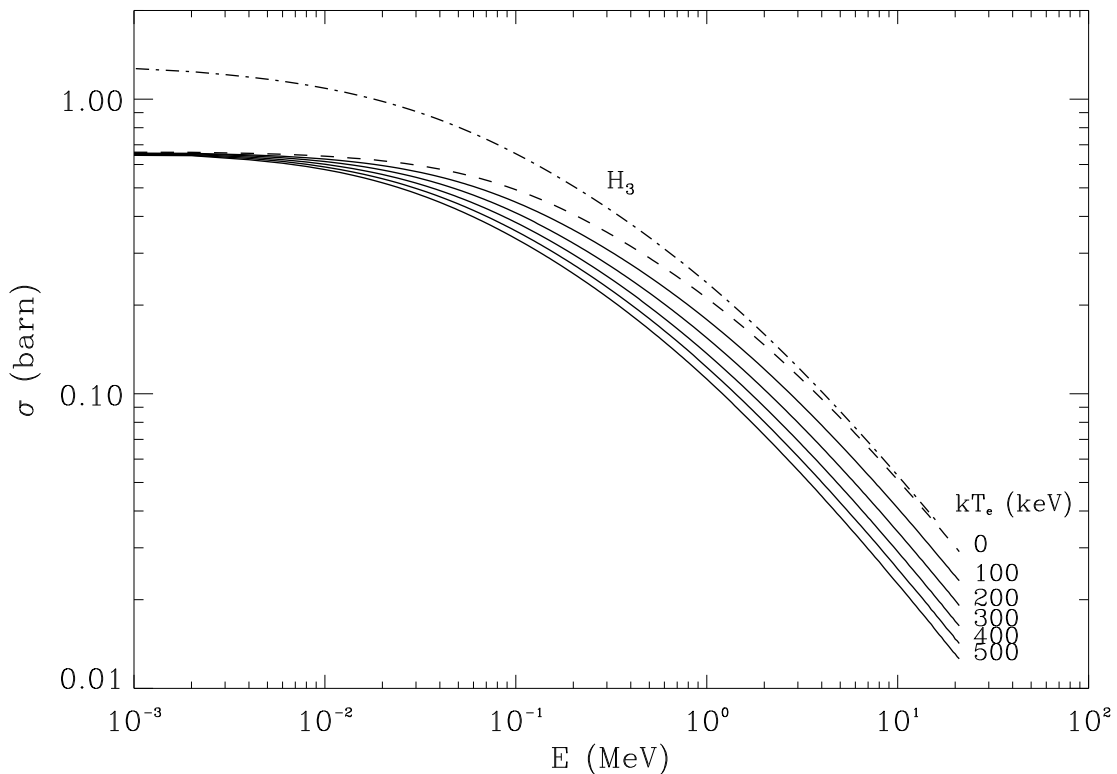


Fig. 1.— Maxwellian averaged Compton scattering cross section for various plasma temperatures, obtained from numerical integration in Equation (10). Also plotted is the maximum effective cross section as a function of photon energy  $H_3(E)$ .

With  $\sigma_a(T_e, E)$  obtained by numerical integration in Eq. (10), we can use the Monte Carlo method to select the free path between two successive scatterings for a photon with energy  $E$ .

$$\int_0^\ell n_e \sigma_a ds = -\ln \xi, \quad (12)$$

where  $\ell$  is the free path to be sampled;  $n_e$  is the electron density and  $\xi$  is a uniform random

number on (0,1). The integration is taken along photon's path length  $s$ . In this section we are only concerned with the isothermal plasmas at temperature  $T_e$  and with uniform density  $n_e$  and leave the discussion about inhomogeneous media to the next two sections. Under this assumption,  $\ell$  can be sampled simply by

$$\ell = -\frac{\ln \xi}{n_e \sigma_a(T_e, E)}. \quad (13)$$

At the location of scattering, an electron is selected to scatter the photon. Its energy factor  $\gamma$  and direction  $\mu = \cos \theta$  with respect to the photon direction are selected according to the distribution

$$f_e(\gamma, \mu) \propto (1 - \mu \sqrt{1 - \gamma^{-2}}) \sigma(\varepsilon) N_e(\gamma), \quad (14)$$

while its azimuthal angle  $\phi$  around the photon direction is selected uniformly on  $(0, 2\pi)$ . The distribution in Eq. (14) is rather complicated because  $\varepsilon$  depends on  $\gamma$  and  $\mu$  as given in Eq. (7). On the other hand, for a thermal plasma,  $N_e(\gamma)$  is given by Eq. (11) and independent of  $\mu$ . In our implementation of the distribution Eq. (14), we use the following algorithm.

1. Generate 2 random numbers  $\xi_1$  and  $\xi_2$  uniformly distributed on (0,1).
2. If  $\Theta \leq 0.01$ ,
  - If  $\xi_2^2 > -e\xi_1 \ln \xi_1$ , go to 1.
  - Else let  $v = \sqrt{-3\Theta \ln \xi_1}$ ,  $\gamma = 1/\sqrt{1 - v^2}$ .
  - Else if  $\Theta \leq 0.25$ ,
    - let  $\gamma = 1 - 1.5\Theta \ln \xi_1$ .
    - If  $\xi_2 H_1 > \gamma \sqrt{\xi_1(\gamma^2 - 1)}$ , go to 1.
  - Else
    - let  $\gamma = 1 - 3\Theta \ln \xi_1$ .
    - If  $\xi_2 H_2 > \gamma \xi_1^2 \sqrt{\gamma^2 - 1}$ , go to 1.
3. Generate  $\mu$  uniform on (-1,1) and  $\xi_3$  uniform on (0,1).
4. Calculate  $\varepsilon$  and then  $\sigma(\varepsilon)$  from  $\gamma$  and  $\mu$  according to Eqs. (7) and (9).
5. If  $\xi_3 H_3 > (1 - \mu \sqrt{1 - \gamma^{-2}}) \sigma(\varepsilon)$ , go to 1.
  - Else accept  $\gamma$  and  $\mu$ .

Here

$$H_1 = a \sqrt{a^2 - 1} \exp\left(-\frac{a-1}{3\Theta}\right),$$

$$a = 2\Theta + 2b \cos\left[\frac{1}{3} \cos^{-1}\left(\Theta \frac{16\Theta^2 - 1}{2b^3}\right)\right] \quad \text{and} \quad b = \sqrt{1/3 + 4\Theta^2}; \quad (15)$$

$$H_2 = a \sqrt{a^2 - 1} \exp\left[-\frac{2(a-1)}{3\Theta}\right],$$

$$a = \Theta + 2b \cos\left[\frac{1}{3} \cos^{-1}\left(\Theta \frac{4\Theta^2 - 1}{4b^3}\right)\right] \quad \text{and} \quad b = \sqrt{1/3 + \Theta^2}; \quad (16)$$

and  $H_3$  is the maximum of the so called “effective cross section”  $\sigma_{\text{eff}} = (1 - \mu\sqrt{1 - \gamma^{-2}})\sigma(\varepsilon)$ .

Several points should be made in the above algorithm. Steps 1 and 2 sample  $\gamma$  using rejection method in terms of the Maxwellian distribution  $N_e(\gamma)$ , which is independent of the photon energy and direction. For low plasma temperature ( $\Theta \leq 0.01$ ) electron velocity  $v$  are sampled according to the non-relativistic Maxwellian distribution. For high temperatures, the separated sampling ( $\Theta \leq 0.25$  and  $> 0.25$ ) is in order to reduce the rejection rates. It should be emphasized that although the expressions of  $H_1$  and  $H_2$  are complicated, these quantities depend on  $\Theta$  alone and therefore need to be calculated once only. They can be calculated outside the scattering loop as long as plasma temperature remains unchanged. The  $\gamma$  values so sampled, together with the isotropically sampled  $\mu$ , represent electrons in the hot plasma at the given temperature. They are subject to another rejection test in the subsequent steps in order to yield the right joint distribution given in Eq. (14), which represents the electrons that actually scatter the photon.

temperature remains unchanged. The  $\gamma$  values so obtained are subject to another rejection test in the subsequent steps together with the isotropically sampled  $\mu$  in order to yield the right joint distribution given in Eq. (14).

The quantity  $H_3$  is not expressible analytically. It depends on incident photon energy  $E$  only and can be determined by maximizing the effective cross section with respect to  $\gamma$  and  $\mu$  for any given  $E$  using numerical methods such as given in Press et al. (1992). In the following, we describe an alternative to the above 2-dimensional maximization methods. We examine the derivative of  $\sigma_{\text{eff}}(\gamma, \mu)$  with respect to  $\mu$

$$\frac{\partial \sigma_{\text{eff}}}{\partial \mu} = - \frac{2E}{m_e c^2} \sqrt{1 - \gamma^{-2}} \frac{dh}{d\varepsilon}, \quad (17)$$

where

$$h(\varepsilon) = \left(1 - \frac{4}{\varepsilon} - \frac{8}{\varepsilon^2}\right) \ln(1 + \varepsilon) + \frac{1}{2} + \frac{8}{\varepsilon} - \frac{1}{2(1 + \varepsilon)^2} \quad (18)$$

is the expression in the square parentheses in Eq. (9). It can be easily verified that

$$\frac{\partial \sigma_{\text{eff}}}{\partial \mu} \leq 0 \quad \text{for } E > 0 \text{ and } \gamma \geq 1 \quad (19)$$

Therefore,  $\sigma_{\text{eff}}(\gamma, \mu)$  is a monotonously decreasing function of  $\mu$ , that is, for given  $\gamma$ ,  $\sigma_{\text{eff}}(\gamma, \mu)$  reaches its maximum at  $\mu = -1$ . Physically, this means that head-on collision between the photon and electron always has the maximum probability. Thus, in order to determine the maximum of  $\sigma_{\text{eff}}$  as a function of  $\gamma$  and  $\mu$ , one only needs to maximize the one dimensional function  $\sigma_{\text{eff}}(\gamma, -1)$ . The maximum of  $\sigma_{\text{eff}}$ , or  $H_3$ , as a function of  $E$  determined in this way is plotted in Figure 1 as the dash-dotted curve. It is seen that for high photon energies, the maximum effective cross section approaches the Klein-Nishina cross section while at low energies it approaches twice the Thomson cross section. The  $H_3$  values for an array of properly spaced  $E$  values can be tabulated and incorporated into the computer codes.

With the selected electron energy and direction represented by  $\gamma$ ,  $\mu$  and  $\phi$  uniform on  $(0, 2\pi)$ , we proceed to determine the energy and direction of the scattered photon. In order to do so,



we simulate Compton scattering in the frame where the electron before scattering is at rest rather than sampling the multivariate distribution of  $E'$ ,  $\mu'$  and  $\phi'$  from Eq. (5). The Lorentz transformation of the photon momentum between this reference frame and the lab frame is given by

$$\mathbf{p}' = \mathbf{p} - p[\gamma v - (\gamma - 1)\hat{\mathbf{p}} \cdot \hat{\mathbf{v}}]\hat{\mathbf{v}}, \quad (20)$$

where  $\mathbf{p}$  and  $\mathbf{p}'$  are photon momentum vectors before and after the transformation;  $\hat{\mathbf{p}}$  and  $\hat{\mathbf{v}}$  are unit vectors of the photon momentum and electron velocity respectively.

In the electron rest frame, we utilize the Monte Carlo method described in §2. The resulting momentum of the scattered photon is then transformed back to the lab frame using the same Eq. (20) with a reversed  $\hat{\mathbf{v}}$ . The energy and direction of the scattered photon obtained in this way automatically satisfy the energy conservation relationship given in Eq. (8).

As a crucial test we ran the program in which low frequency photons were allowed to scatter in an infinite plasma at a given temperature for a sufficiently long time. It was expected that the photon energy should approach the Wien distribution at the given plasma temperatures. One example of such evolution, the photon energy distribution recorded at various times in a plasma of  $kT_e = 200$  keV are shown in Figure 2. It does approach the Wien form.

#### 4. Comptonization in Multi-Zone Media

If Comptonization takes place in a medium which is divided into several zones each with different electron temperatures and density distributions, one has to take into consideration the boundaries between these zones in addition to the scattering free paths and the boundary of the entire medium.

In general, suppose a photon, after initiation or scatterings, is located in the medium at  $(x_0, y_0, z_0)$  with a direction  $(\omega_1, \omega_2, \omega_3)$ . The next position where the photon will scatter, if there were no boundaries, is given by

$$\begin{cases} x_1 = x_0 + \ell\omega_1 \\ y_1 = y_0 + \ell\omega_2 \\ z_1 = z_0 + \ell\omega_3, \end{cases} \quad (21)$$

where  $\ell$  is sampled according to Eq. (13), in which  $n_e$  and  $T_e$  should be understood as the electron density and temperature in the present zone. With the existence of boundaries,  $(x_1, y_1, z_1)$  could be in the neighboring zone or outside of the medium. In this case, one has to calculate the distances  $s_i$  from  $(x_0, y_0, z_0)$  to various boundaries  $B_i$ , ( $i = 1, \dots, N$ ), where  $N$  is the number of boundaries surrounding the zone under consideration.  $s_i$  can be obtained by solving the equations describing the  $i$ th boundary

$$B_i(x, y, z) = 0, \quad i = 1, \dots, N \quad (22)$$

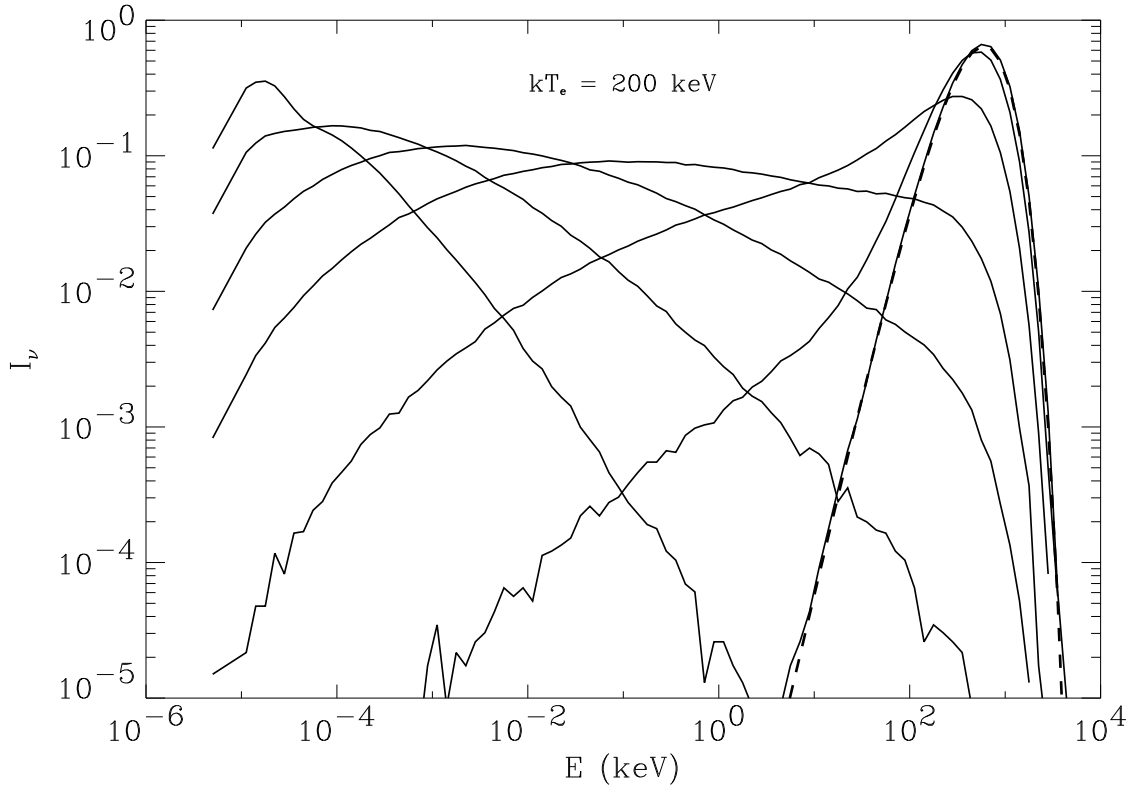


Fig. 2.— The evolution of photon energy spectrum from a blackbody at  $0.511 \times 10^{-2}$  eV towards equilibrium with a plasma at  $kT_e = 200$  keV. The seven spectra (solid curves) are “snapshots” at times  $t = 1, 3, 6, 10, 18, 30, 70$  Thomson mean free time. Also plotted (dashed curve) is the Wien spectrum at temperature 200 keV.

where

$$\begin{cases} x = x_0 + s_i \omega_1 \\ y = y_0 + s_i \omega_2 \\ z = z_0 + s_i \omega_3. \end{cases} \quad (23)$$

If  $\ell$  is smaller than any of  $s_1, \dots, s_N$  so obtained, the photon will remain in the same zone and scatter at the location  $(x_1, y_1, z_1)$  on electrons at local temperature  $T_e$ . But if  $s_j$  is the minimum among  $\ell$  and  $s_1, \dots, s_N$ , the photon will hit the boundary  $B_j$ . In this case one has to replace the photon on the boundary at  $(x, y, z)$  determined by Eq. (23) with  $i = j$ . With the new position on the boundary as  $(x_0, y_0, z_0)$ , one can begin another round of free path sampling with  $n_e$  and  $T_e$  of the zone the photon is entering but keeping the photon energy and direction unchanged.

In the study of Gamma-ray spectra of Cygnus X-1 (Ling et al. 1997), we developed a model where photons scatter in a two-layered spherical plasma consisting of a high-temperature core and a cooler corona. The model was first proposed by Skibo and Dermer (1995) to interpret the

X-ray spectral hardening at high energies observed in AGNs. The boundary of the inner core is a sphere of radius  $R_i$  while the boundaries of the outer shell are two spheres with radii  $R_i$  and  $R_o$  respectively. For a photon in the core, the equation for the distance  $s_1$  to its boundary is

$$s_1^2 + 2(\mathbf{r}_0 \cdot \hat{\omega})s_1 - (R_i^2 - r_0^2) = 0, \quad (24)$$

where  $\mathbf{r}_0 = (x_0, y_0, z_0)$  is the position vector of the photon;  $\hat{\omega} = (\omega_1, \omega_2, \omega_3)$ . Similarly, the equations for a photon in the outer shell are

$$\begin{cases} s_1^2 + 2(\mathbf{r}_0 \cdot \hat{\omega})s_1 - (R_i^2 - r_0^2) = 0 \\ s_2^2 + 2(\mathbf{r}_0 \cdot \hat{\omega})s_2 - (R_o^2 - r_0^2) = 0 \end{cases}. \quad (25)$$

Thus we have the following algorithm:

If  $r_0 < R_i$ ,

Let  $\delta = (\mathbf{r}_0 \cdot \hat{\omega})^2 + (R_i^2 - r_0^2)$  and  $s_1 = \sqrt{\delta} - (\mathbf{r}_0 \cdot \hat{\omega})$ .

If  $\ell < s_1$ , scatter at  $\mathbf{r}_1 = \mathbf{r}_0 + \ell\hat{\omega}$ .

Else reach boundary at  $\mathbf{r}_1 = \mathbf{r}_0 + s_1\hat{\omega}$ .

Else if  $r_0 < R_o$ ,

Let  $\delta = (\mathbf{r}_0 \cdot \hat{\omega})^2 + (R_i^2 - r_0^2)$ .

If  $\delta \geq 0$  and  $(\mathbf{r}_0 \cdot \hat{\omega}) < 0$ ,

Let  $s_1 = -\sqrt{\delta} - (\mathbf{r}_0 \cdot \hat{\omega})$ .

If  $\ell < s_1$ , scatter at  $\mathbf{r}_1 = \mathbf{r}_0 + \ell\hat{\omega}$ .

Else reach boundary at  $\mathbf{r}_1 = \mathbf{r}_0 + s_1\hat{\omega}$ .

Else

Let  $\delta = (\mathbf{r}_0 \cdot \hat{\omega})^2 + (R_o^2 - r_0^2)$  and  $s_2 = \sqrt{\delta} - (\mathbf{r}_0 \cdot \hat{\omega})$ .

If  $\ell < s_2$ , scatter at  $\mathbf{r}_1 = \mathbf{r}_0 + \ell\hat{\omega}$ .

Else escape.

Whenever the photon crosses the inner boundary, the plasma density and temperature should be switched while the photon energy and direction kept unchanged.

In figure 3, we present the result of such a calculation (solid curve) together with the observational data (Ling et al. 1997) it was intended to fit. The data was from the blackhole candidate Cygnus X-1 observed by the detector BATSE on board satellite Compton Gamma-Ray Observatory. The fitting spectrum was obtained from a calculation with the two-layer model described above, where temperature is  $kT_e = 230$  keV for the inner core and 50 keV for the outer shell. The two zones are assumed to have the same electron density and the inner core has a radius 0.36 in units of Thomson mean free path, while the outer-shell radius is 1.3. The initial photons have a blackbody temperature of 0.5 keV and injected into the medium from outside. For comparison the best fit one can achieve by a single-zone plasma model is also presented (dashed curve). The model consists of a plasma sphere of radius 1.35 at  $kT_e = 85$  keV. The reduced  $\chi^2$

value is 2.6 for the single-temperature model as compared to 1.0 for the double-layer model. It is seen that by adding a hot central core to the Comptonization medium, the fit to the high-energy part of the observed spectrum is significantly improved.

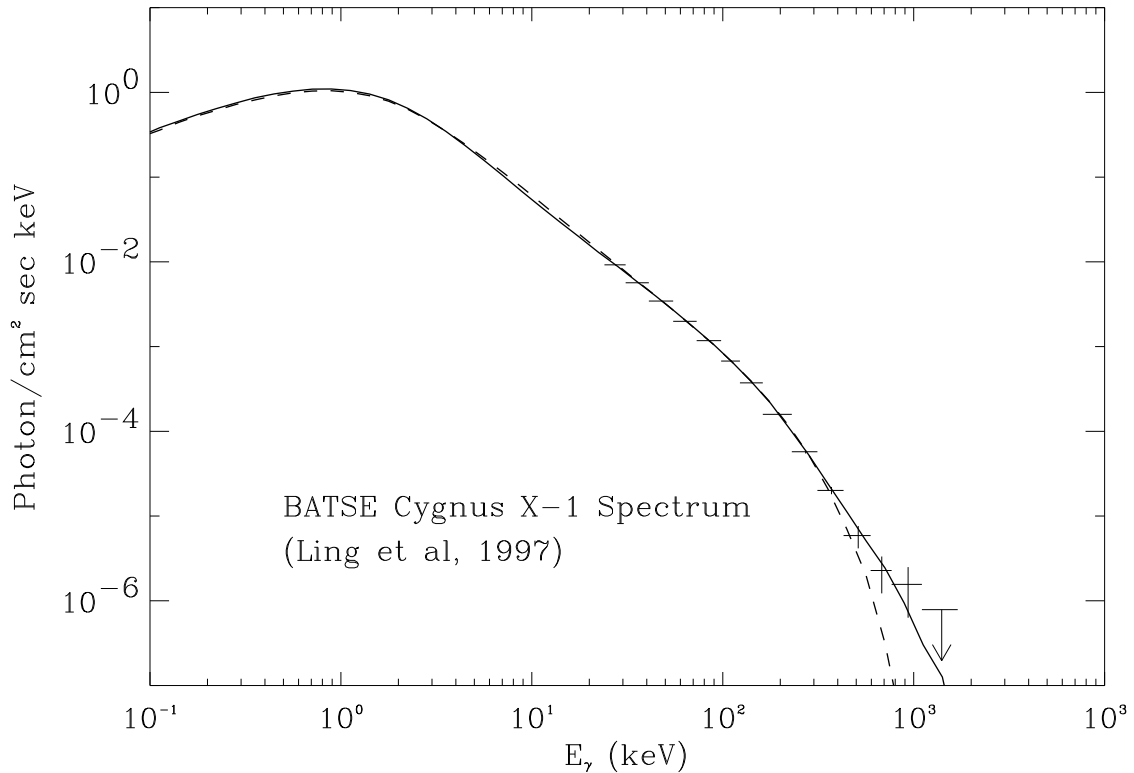


Fig. 3.— The energy spectra resulting from the double-layer Comptonization media (solid curve) and single-temperature sphere (dashed curve). Both spectra are intended to fit the observational data from the blackhole candidate Cygnus X-1 (Ling et al, 1997).

## 5. Comptonization in Isothermal Media with Non-Uniform Density

The media we considered so far are uniform, at least regionally, in density. It was found necessary to investigate the Comptonization in the media with non-uniform density profiles (Kazanas et al, 1997). In this section, we present the treatment of two spherically symmetrical configuration commonly found in astrophysical environment, one with electron density varying as  $\rho^{-1}$  and the other as  $\rho^{-3/2}$ , where  $\rho$  is the distance from the sphere center. The latter case represents the density profile of a gas free-falling onto a central accreting object under gravitational force (e.g. Narayan & Yi 1994), while the former represents that of an accreting gas with viscosity due to the interaction between the gas and the outgoing photons (Kazanas et al, 1997).

With density  $n_e$  varying along the photon's path length  $s$ , the integration in Eq. (12) should be written as

$$I = \int_0^\ell n_e(s) \sigma_a ds, \quad (26)$$

where the dependence of  $n_e$  on  $s$  is given by

$$n_e(s) = \begin{cases} \frac{n_0 \rho_0}{\sqrt{r_0^2 + s^2 + 2sr_0\nu}} & \text{for } \rho^{-1} \text{ profile,} \\ \frac{n_0 \rho_0^{3/2}}{(r_0^2 + s^2 + 2sr_0\nu)^{3/4}} & \text{for } \rho^{-3/2} \text{ profile,} \end{cases} \quad (27)$$

where  $\rho_0$  is the radius of the sphere within which the density profiles break down;  $n_0$  is the electron density at this radius;  $\nu = (\mathbf{r}_0 \cdot \hat{\omega})/r_0$ ;  $\mathbf{r}_0$  is the photon's position vector originated from the sphere center and  $\hat{\omega}$  its travel direction.

Substitute  $n_e(s)$  in Eq. (27) into Eq. (26) and we obtain the integration for  $\rho^{-1}$  profile

$$I = n_0 \rho_0 \sigma_a \ln \left[ \frac{\ell - r_0 \nu + \sqrt{\ell^2 + r_0^2 + 2\ell r_0 \nu}}{r_0(1 - \nu)} \right]. \quad (28)$$

Eq. (12) then becomes  $I = -\ln \xi$ . Solving this equation for  $\ell$ , we obtain

$$\ell = r_0 \frac{(1 + \nu)\eta^2 + 2\nu\eta - (1 - \nu)}{2\eta}, \quad (29)$$

where  $\eta = \exp(-\ln \xi / n_0 \rho_0 \sigma_a)$ . Once a uniform random  $\xi$  is selected on  $(0, 1)$ ,  $\ell$  is determined by Eq. (29).

For  $\rho^{-3/2}$  density profile, the counterpart of Eq. (28) is

$$I = n_0 \rho_0 \sigma_a \sqrt{\frac{2\rho_0}{r_0 \sin \vartheta}} \left[ F(\varphi_\ell, \frac{1}{\sqrt{2}}) - F(\varphi_0, \frac{1}{\sqrt{2}}) \right], \quad (30)$$

where  $F(\varphi, k)$  is the Legendre elliptic integral of the 1st kind;  $\sin \vartheta = \sqrt{1 - \nu^2}$ ;  $\varphi_0$  and  $\varphi_\ell$  are given by

$$\begin{cases} \cos \varphi_0 = (1 + u_0^2)^{-1/4} \\ \cos \varphi_\ell = (1 + u_\ell^2)^{-1/4}, \end{cases} \quad (31)$$

and

$$\begin{cases} u_0 = \frac{\cos \vartheta}{\sin \vartheta} \\ u_\ell = \frac{\ell + r_0 \cos \vartheta}{r_0 \sin \vartheta}. \end{cases} \quad (32)$$

Substituting the integration into Eq. (12), we obtain

$$F(\varphi_\ell, \frac{1}{\sqrt{2}}) = F(\varphi_0, \frac{1}{\sqrt{2}}) - \frac{\ln \xi}{n_0 \rho_0 \sigma_a} \sqrt{\frac{r_0 \sin \vartheta}{2\rho_0}}, \quad (33)$$

where the right-hand side is a function of known variables. Call it  $f(\xi, r_0, \vartheta)$ . Solve Eq. (33) and we obtain

$$\cos \varphi_\ell = \text{cn}(f, \frac{1}{\sqrt{2}}), \quad (34)$$

where  $\text{cn}(f, k)$  is the Jacobian elliptic function, which is the inverse of the elliptic integral  $F(\varphi_\ell, k)$ . Computer routines for both elliptic integral and Jacobian elliptic function are available in many mathematical libraries (e.g. Press et al, 1992). Finally,  $\ell$  can be obtained from Eqs. (31) and (32)

$$\ell = r_0 \sin \vartheta \sqrt{\text{cn}^{-4}(f, \frac{1}{\sqrt{2}}) - 1} - r_0 \cos \vartheta. \quad (35)$$

Once  $\ell$  is available, one can use the algorithms described in the previous section to determine if the photon scatters, escapes or hits the boundary.

We used  $\ell$  given in Eqs. (29) and (35) to study the Comptonization in a two-layer spherical model similar to that in the last section but with the outer layer having a  $\rho^{-1}$  or  $\rho^{-3/2}$  density profile. Specifically, we assume the density in the outer shell is given by Eq. (27) with  $\rho_0 = R_i$  and the density of the inner core is constant  $n_+$ . It is found that the energy spectrum of the X-rays emerging from such system is different from a uniform sphere with the same optical depth (Kazanas et al, 1997). More importantly, with the decreasing density profiles, the outer layer, or the “atmosphere” can extend to a distance much greater than the size a uniform system with the same optical depth can do, giving rise to the time variation properties on a much greater time scale.

As an example, we show in Figure 4 two light curves, or the time-dependent fluxes, for X-ray photons escaping from two such core-atmosphere systems, one with  $\rho^{-1}$  and the other with  $\rho^{-3/2}$  density profile for the atmospheres. For both density profiles, the temperature is 50 keV in the atmosphere as well as in the core; the total optical depth is 2 in terms of Thomson scattering and the radius of the inner cores is assumed to be  $2 \times 10^{-4}$  light seconds. The core density  $n_+$  is slightly different from each other:  $1.6 \times 10^{17}$  and  $1.68 \times 10^{17} \text{cm}^{-3}$  for  $\rho^{-1}$  and  $\rho^{-3/2}$  profiles respectively. For the outer atmospheres,  $n_0$  in Eq. (27) are  $0.4 \times 10^{17} \text{cm}^{-3}$  and  $1.68 \times 10^{17} \text{cm}^{-3}$  respectively. As a result the radii of the systems are 1.01 and 2.63 light seconds respectively.

Photons of a blackbody spectrum at temperature 2 keV are injected at the center into the system. The Comptonized photons in the energy range 10 – 20 keV are collected in terms of their escape time, producing the light curves displayed in the figure. It is seen that these light curves are power-laws extending to the order of seconds followed by exponential cutoffs. The indices of the power-law are roughly 1 and 3/2 respectively, which was explained in Kazanas et al (1997). This

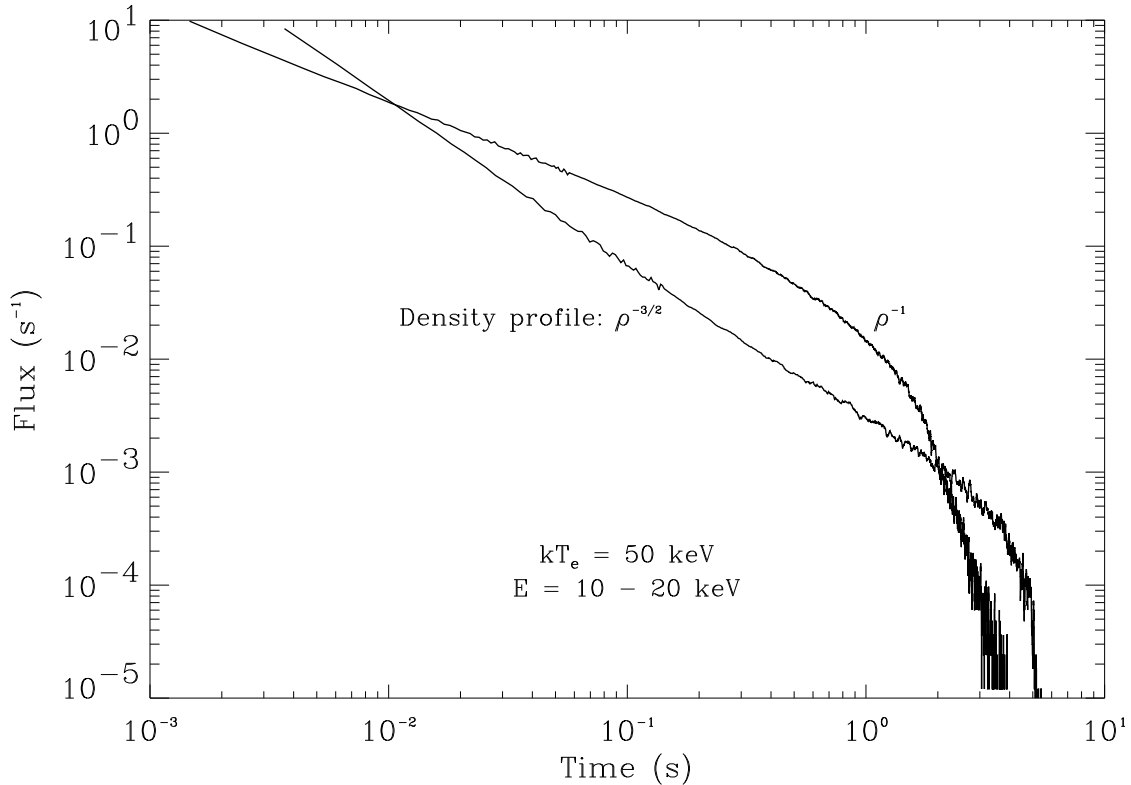


Fig. 4.— The light curves resulting from the core-atmosphere models. The atmospheres have  $\rho^{-1}$  and  $\rho^{-3/2}$  density profiles respectively.

temporal behavior is greatly different from the light curves from a uniform system, which decay exponentially from the very beginning of the emissions (Hua & Titarchuk, 1996). In addition, for a uniform system of the similar optical depth and an electron density of the order of  $10^{16}$  or  $10^{17} \text{ cm}^{-3}$ , the characteristic decay time of the light curves will be  $\sim 1$  millisecond. The implication of the prolonged power-law light curves resulting from the extended atmosphere models for the interpretation of the recent X-ray observational data is discussed elsewhere (Kazanas et al. 1997, Hua et al. 1997).

## 6. Summary

We have shown that analytical method has intrinsic limitations in dealing with Comptonization problem and Monte Carlo simulation provides a useful alternative. We have introduced an efficient Monte Carlo method that can solve the Comptonization problem in a truly relativistic way. The method was further expanded to include the capabilities of dealing with Comptonization in the

media where electron density and temperature vary discontinuously from one region to the other and in the isothermal media where density varies continuously along photon paths. In addition to the examples given above for its application, the method was also used in the investigation of Compton scattering of gamma-ray photons in the accretion disks near black hole candidates (Lingenfelter & Hua, 1991) and in the Earth's atmosphere and the spacecraft material (Hua & Lingenfelter, 1993).

The author would like to thank R. E. Lingenfelter and R. Ramaty for their long-term support and encouragement in the past decade during which the technique described here was developed. The author also wants to thank J. C. Ling, L. Titarchuk and D. Kazanas for valuable discussions and NAS/NRC for support during the period of this study.

## REFERENCES

- Akhiezer, A.I. & Berestetskii V.B. 1969 Quantum Electrodynamics, Nauka, Moscow.
- Gorecki, A. & Wilczewski, W. 1984, *Acta Astronomica*, 34 141.
- Hua, X.-M. 1986, Ph.D. thesis, University of California, San Diego.
- Hua, X.-M. & Lingenfelter, R.E. 1993, *ApJ*, 416, L17.
- Hua, X.-M. & Lingenfelter, R.E. 1993, *Proceedings of Compton Observatory Symposium*, 927.
- Hua, X.-M., Kazanas, D. & Titarchuk L. 1997, *ApJ*, 482, in press.
- Hua, X.-M. & Titarchuk, L. 1995, *ApJ*, 449, 188.
- Hua, X.-M. & Titarchuk, L. 1996, *ApJ*, 469, 280.
- Kahn, H. 1954, *Application of Monte Carlo (AECU-3259)*.
- Kazanas, D., Hua, X.-M. & Titarchuk, L. 1997, *ApJ*, 480, 735.
- Kompaneets, A.S. 1956, *Zh. Eksper. Teoret. Fiz.*, 31, 876 (*Soviet. Phys.-JEPT*, 4, 730 [1957]).
- Landau, L. D. & Lifshits, E. M. 1976 *The Classical Theory of Fields* (4th ed., Pergamon).
- Ling, J. C., Wheaton, Wm. A., Wallyn, P., Mahoney, W. A., Paciesas, W. S., Harmon, B. A., Fishman, G. J., Zhang, S. N. & Hua, X.-M. 1997, *ApJ*, in press.
- Lingenfelter, R.E. & Hua, X.-M. 1991, *ApJ*, 381, 426.
- Narayan, R. & Yi, I., 1994, *ApJ*, 428, L13.
- Payne, D.G. 1980, *ApJ*, 237, 951.
- Pei, L.-C. 1979, *KEJI*, 4, 374 (in Chinese).
- Pozdnyakov, L.A., Sobol, I.M. & Sunyaev, R.A. 1983 in *Astrophysics and Space Physics Reviews*, Soviet Scientific Reviews 2, 189, ed. R.A. Sunyaev.
- Press, W.H., Teukolsky, S.A., Vetterling, W.T. & Flannery, B.P. 1992, *Numerical Recipes* (University Press, Cambridge).



- Ripley, B. D. 1987, *Stochastic Simulation* (John Wiley & Sons, New York).
- Skibo, J.G. & Dermer, C.D., *ApJ*, 455, L25, 1995.
- Skibo, J.G., Dermer, C.D., Ramaty, R. & McKinley, J.M. 1995, *ApJ*, 446, 86.
- Stern, B.E., Begelman, M.C., Sikora, M. & Svensson, R. 1995, *MNRAS*, 272, 291.
- Sunyaev, R. A. & Titarchuk, L.G. 1980, *A&A*, 86, 121.
- Titarchuk, L. 1994, *ApJ*, 434, 570.